

Superconducting proximity effect in epitaxial Al-InAs heterostructures

William Mayer¹, Joseph Yuan¹, Kaushini S. Wickramasinghe^{1,2},

Tri Nguyen³, Matthieu C. Dartiailh¹, and Javad Shabani¹

¹Center for Quantum Phenomena, Department of Physics, New York University, NY 10003, USA

²Department of Physics, University of Maryland, College Park, MD 20742, USA

³Department of Physics, City College of City University of New York, New York, NY 10031, USA

(Dated: May 5, 2022)

Semiconductor-based Josephson junctions provide a platform for studying the proximity effect due to possibility of tuning junction properties by gate voltage and large-scale fabrication of complex Josephson circuits. Recently Josephson junctions using InAs weak link with epitaxial aluminum contact have improved the product of normal resistance and critical current, $I_c R_N$, in addition to fabrication process reliability. Here we study similar devices with epitaxial contact and find large supercurrent and substantial product of $I_c R_N$ in our junctions. However we find a striking difference when we compare these samples with higher mobility samples in terms of product of excess current and normal resistance, $I_{ex} R_N$. The excess current is negligible in lower mobility devices while it is substantial and independent of gate voltage and junction length in high mobility samples. This indicates that even though both sample types have epitaxial contacts only the high-mobility one has a high transparency interface. In the high mobility short junctions, we observe record values of $I_c R_N / \Delta \sim 2.2$ and $I_{ex} R_N / \Delta \sim 1.5$ in semiconductor weak links.

Recently, realizing transparent contact in superconductor-semiconductor (S-Sm) systems has become the focus of renewed theoretical and experimental attention partly because of the potential applications in spintronics, topological superconductivity [1, 2] and superconducting quantum computation [3–5]. Generally materials considered for S-Sm systems such as GaAs two-dimensional electron gas (2DEG) [6] contacted with either aluminum or niobium based superconductors have had high quality 2DEG's but suffered from imperfect interfaces due to the presence of a Schottky barrier. Narrow bandgap materials such as InAs and InSb have been studied due to the potential for transparent metallic interfaces [7], first using 2DEG's [8–10] and more recently using nanowires [11]. Recently it has been shown that epitaxial contacts to nanowires and near surface quantum wells can improve the proximity effect in Josephson junctions [12, 13]. The figure of merit $I_c R_N$, where I_c is the critical current and R_N is normal resistance, normalized by Δ_0/e up to 0.7 has been achieved. These improvements over earlier studies [14] were associated with the in-situ growth of epitaxial superconducting contact. These epitaxial contacts can be made only to electrons confined near surface where by design mobility is dominated by surface scattering. Depending on the application, in some cases high electron mobility is desired [15, 16] and in other cases control over the induced gap is called for [17]. It was determined in near surface 2DEGs, 10-nm thick top layer of $\text{In}_{0.81}\text{Ga}_{0.19}\text{As}$ can achieve both [13, 18].

In this work, we study the electronic transport properties and their connection to Josephson effect properties in InAs structures with Al epitaxial contact. We study these properties in samples of different bare mobilities (not gated) to not only compare the nature of the interface formed by in-situ epitaxial growth but also the effect of the 2DEG quality. These hybrid system can be charac-

terized by study of the products $I_c R_N$ and $I_{ex} R_N$, where I_{ex} is the excess current, as figures of merit for induced gap and interface transparency. We find that 2DEG mobility and the inferred interface transparency seem to be closely related, possibly due to the fact that the mobility of surface 2DEG has been found to be dominated by surface scattering [18]. This implies that the same impurities affecting the 2DEG mobility will also dominate degradation of the interface in the case of in-situ epitaxial growth, which would otherwise produce a transparent interface. In higher mobility samples we study $I_c R_N$ for different junction lengths, temperatures and gate voltage where the analysis is in agreement with a fully transparent metallic interface. We also find that $I_{ex} R_N$ is independent of JJ length and applied gate voltage in contrast to previous studies [19–21]. In our high mobility 100 nm short junction we report $I_c R_N / \Delta$ values up to 2.2 and $I_{ex} R_N / \Delta \sim 1.5$.

The samples were grown on semi-insulating InP (100) substrates. The quantum well consists of a 4 nm layer of InAs grown on a 6 nm layer of $\text{In}_{0.81}\text{Ga}_{0.19}\text{As}$. Since coupling the 2DEG to a superconductor is the main requirement, the charge distribution at the semiconductor metal interface has to be finite. To satisfy this condition we grow a 10nm $\text{In}_{0.81}\text{Ga}_{0.19}\text{As}$ layer on the InAs which has been found to produce an optimal interface while maintaining relatively high 2DEG mobility [18]. After the quantum well is grown, the substrate is cooled to promote the growth of epitaxial Al (111). Wafer A and B are grown with identical nominal structure. The difference in arsenic overpressure (or equivalently III/V ratio) during the growth of lattice-mismatched buffer results in different misfit dislocations and varied roughness. Atomic force microscopy images of samples are shown in Figure 1(a) and 1(b). Images show variation of minimum and maximum topography within a $34 \mu\text{m}$ square window to be approximately 9 nm for sample A and 7 nm for

sample B. It should be noted that these images are taken from the full structure with top Al layer. The roughness is similar when Al is selectively removed indicating roughness is due primarily to underlying semiconductor structure, not Al.

To determine the mobility and density, selective wet etching techniques are used to remove the top Al layer to measure both longitudinal and transverse resistances in a van der Pauw geometry. The magnetoresistance for the two samples we will consider in this paper are plotted in Figures 1(c) and 1(d). Josephson junctions are fabricated with electron beam lithography. Devices are gated using 50 nm of AlO_x deposited by ALD followed by lithographically defined Ti/Au gates. All studied junctions have a 4 μm width (W) with varying gap lengths (L) and are measured in a 4-point geometry. Measurements are performed in a dilution fridge with mixing chamber temperature of 7 mK and an estimated electron temperature of 20 mK.

When considering the properties of these InAs JJ's, both transparency of the InAs-Al interface and scattering within the 2DEG need to be considered. Scattering in the 2DEG determines whether transport through the junction is diffusive or ballistic, generally characterized by the mean free path l_e in comparison with junction length, L . Magnetotransport for samples shown in Figure 1 yields mean free paths $l_e^A = 87$ nm and $l_e^B = 201$ nm. We fabricate multiple junctions on samples taken from wafer A and B. With JJ lengths ranging from 50 nm to 1 μm , mean free paths of this order indicate transport is between the diffusive and ballistic limits. The T_c of both Al thin films is measured and found to be $T_c^A = 1.53$ K and $T_c^B = 1.48$ K, superscript denotes the sample. Using the relation $\Delta_{\text{Al}} = 1.75k_B T_c$ we find $\Delta_{\text{Al}}^A = 231$ μV and $\Delta_{\text{Al}}^B = 223$ μV with the variation being attributed to slightly different Al film thicknesses. This is supported by perpendicular magnetic field measurements yielding critical fields of $B_c^A = 164$ mT and $B_c^B = 96$ mT. From Δ_{Al} we can estimate the superconducting coherence length in our samples given by $\xi_0 = \hbar v_F / (\pi \Delta)$, which yields $\xi_0^A = 635$ nm and $\xi_0^B = 774$ nm for respective samples. From this we expect all devices to approach the dirty limit ($\xi_0 \gg l_e$). This implies we should also consider the dirty coherence length $\xi_{0,d} = \sqrt{\xi_0 l_e}$ which yields $\xi_{0,d}^A = 235$ nm and $\xi_{0,d}^B = 394$ nm. A summary of devices fabricated on both wafer A and B are shown in Fig. 2.

The standard figure of merit for JJ is $I_c R_N$. It should be noted that experimentally there is a distinction between I_c and the measured switching current of a junction. In an ideal system these quantities would be identical but it is commonly seen that finite temperature or noise can cause the junction to prematurely switch. This leads to measuring an observed switching current lower than I_c . For simplicity in the analysis, we assume that they are equal in our devices while knowing this can lead to an underestimation of our I_c . The I_c requires coherent charge transport across the semiconducting region. The critical current can also be related to the gap by

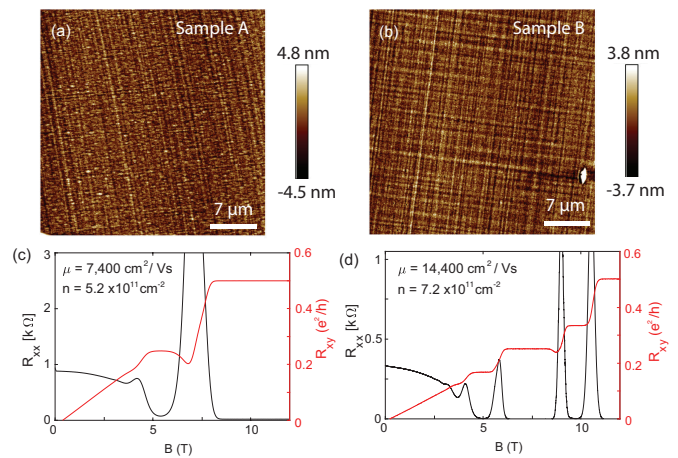


FIG. 1: (Color online) Atomic force microscopy image of (a) sample A and (b) sample B. (c) Longitudinal (black) and Hall (red) resistance shown as a function of magnetic field for sample A and (d) similarly for sample B at 20 mK.

the formula $I_c R_n = \alpha \Delta_0 / e$. From Fig. 3 (a,b) insets we find $I_c R_n^A = 135$ μV and $I_c R_n^B = 486$ μV . These values can be compared to theoretical values for junctions in the short diffusive and ballistic limits, for which α are $1.32(\pi/2)$ and π respectively [24, 25] when JJs are deep in ballistic ($l_e \gg L$) or diffusive regime ($L \gg l_e$). For sample B we find $I_c R_n$ is 69% of the ballistic limit and 105% of the diffusive limit. In contrast the results for sample A are 17% of the ballistic limit and 28% of the diffusive limit. From Fig. 2 it is clear that 100 nm JJ in Sample B is in short ballistic regime while 100 nm JJ in sample A is in short diffusive regime.

High interface transparency corresponds to a high probability of Andreev reflection at the interface. Since the Sm extends under the S regions, the interface between Sm and S should be highly transparent due to the large area of contact and in-situ epitaxial Al growth [26]. The Andreev process that carries the supercurrent across the Sm region is characterized by the excess current (I_{ex}) through the junction $I_{ex} = I - V/R_N$ [27]. Excess current does not require coherent charge transport across the junction as it follows simply from charge conservation at the S-Sm interfaces. This allows for the excess current to be calculated by extrapolating from the high current normal regime to zero voltage as shown in Figures 3(a) and 3(b) with dotted lines. The excess current in samples A and B are found to be $I_{ex}^A = 20$ nA and $I_{ex}^B = 3.5$ μA respectively for 100 nm JJ.

When considering interface quality the more relevant quantity is the product of I_{ex} and the normal resistance (R_N). The product $I_{ex} R_N$ can be compared to the superconducting gap with the relation $I_{ex} R_N = \alpha' \Delta_0 / e$. In the case of a fully transparent S-Sm interface $\alpha' = 1.467$ for a diffusive junction [28] and $\alpha' = 8/3$ for a ballistic junction [27]. For samples A and B, $I_{ex} R_N^B = 30$ μV and $I_{ex} R_N^A = 340$ μV . Comparing these to the ballistic and diffusive limits we see that our values

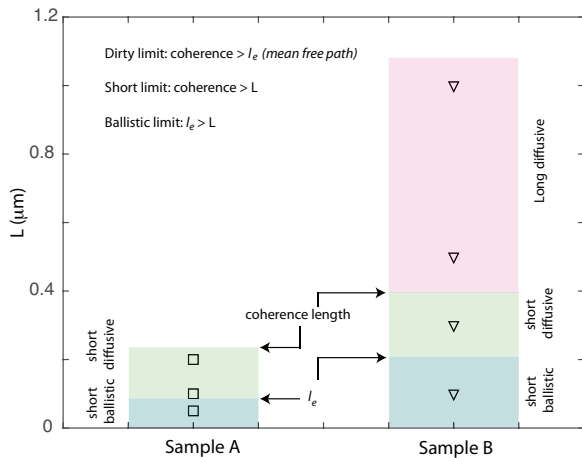


FIG. 2: (Color online) Summary of devices fabricated on two samples from two wafers. The relevant length scale are junction length, L , coherence length and mean free path, l_e . All samples are in the dirty limit.

are 57% of ballistic limit and at 104% actually slightly exceeds the diffusive value for a 100 nm JJ on sample B. Sample A is at only 5% for ballistic and 9% of diffusive limit despite the mean free path of the devices being separated by only approximately a factor of two. As indicated previously, for $L = 100$ nm the ratio L/l_e is close to unity. Consequently for a fully transparent interface we would expect $I_{ex}R_N$ to be between the two limiting cases as is observed for sample B.

This large difference between figure of merits for sample A and B indicates that the scattering at interfaces is quite different despite both samples having in-situ epitaxial contacts. While the mobility only differs by a factor of two the much larger difference in $I_{ex}R_N$ indicates it is not simply the increased scattering in the 2DEG that is responsible for the decrease. Thus one can conclude that I_c is mainly sensitive to any scattering in the 2DEG, while I_{ex} is sensitive to scattering at the interface and independent of scattering processes in the 2DEG. We should note that in near surface 2DEGs it could be that interface transparency and mobility are coupled. It has been shown in these materials that the dominant scattering mechanism is surface scattering [18]. If scatterers are present on the surface they will also affect the interface to the metal, making mobility a good proxy for interface transparency, at least for the ranges of mobility studied in this paper.

The values for $I_{ex}R_N$ and I_cR_N indicate sample B has both a highly transparent S-Sm interface and a high quality 2DEG which can support coherent transport in a 100 nm JJ. Alternatively sample A has drastically lower values despite the same in-situ epitaxial contacts. So while both samples show robust dc Josephson effect made possible by in-situ epitaxial contacts, this result leads us to conclude that in-situ epitaxy does not necessarily lead to transmission near unity. This emphasizes the importance of growing high mobility surface quantum wells

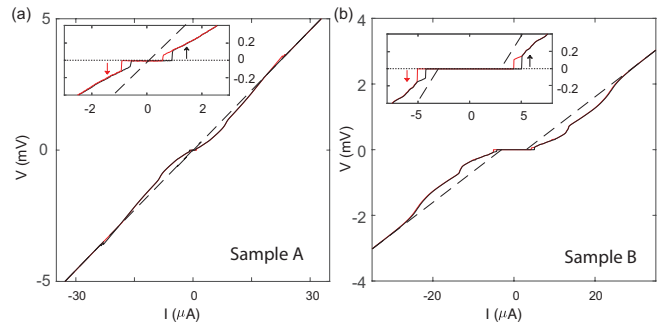


FIG. 3: (Color online) Voltage-current curve for 100 nm Al-InAs JJ (a) on sample A (b) and sample B at 20 mK. The inset shows near zero bias data where the current switches. Higher bias data show the linear extrapolation from normal state (crossed checked with finite magnetic field) to zero voltage yielding I_{ex} .

for applications that require transparent S-Sm interfaces such as the search for topological superconductivity.

The length of the 2DEG channel between superconducting electrodes, L , can be varied as shown in Fig. 2. Figure 4(a) shows the products I_cR_N for both samples on junctions up to $1 \mu m$ using cross symbols. I_cR_N decreases with junction length. From the theory for long junctions where $I_cR_N = I_{c0}R_N e^{-(L/\xi_{0,d})}$ [29], we plot the theoretical expectation as the solid line (in range of 400 nm up to $1 \mu m$) with prefactor (zero length intercept) found to be $I_{c0}R_N \sim 900 \mu V$ while for small values of L we expect $I_cR_N = \pi\Delta_0/e \sim 700 \mu V$, the short ballistic limit.

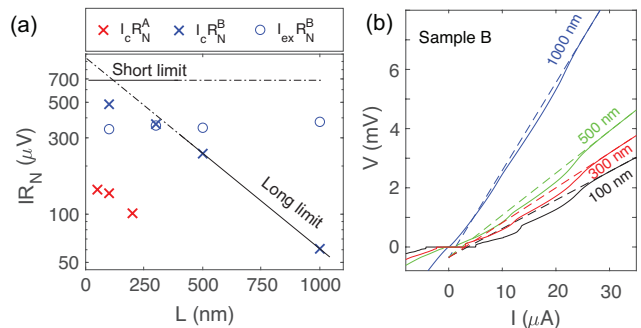


FIG. 4: (Color online) (a) Semi-log plot of dependence of I_cR_n on junction length for sample A (red crosses) and sample B (blue crosses) compared to theoretical exponential dependence (solid black line). Also shown are values of $I_{ex}R_n$ (filled blue circles) as a function of junction length for sample B. (b) VI curves for JJ on sample B of various lengths. Dashed line shows linear extrapolation of slope at high biases to zero voltage yielding I_{ex} .

Figure 4 also shows $I_{ex}R_N$ for sample B. The values for sample A (not shown) are trivially constant. As previously stated for this sample even at $L = 100$ nm, $I_{ex} = 20$ nA and remains small for all measured lengths. In contrast with I_cR_n length dependence we see no sig-

nificant change in $I_{ex}R_N$ over the studied lengths [19–21]. This can also be seen in Figure 4(b), since the y-intercepts of the extrapolated linear fits to the VI curves are simply $I_{ex}R_N$. A decrease in $I_{ex}R_N$ with JJ length has always previously been observed experimentally in both diffusive and ballistic junctions on various materials. It has been shown theoretically that in ballistic junctions $I_{ex}R_N$ will only remain constant with junction length for highly transparent interfaces [30].

The product I_cR_N can be directly varied by changing the Al superconducting gap by increasing temperature. Figure 5a shows the temperature dependence of I_cR_N of 100 nm JJs for sample A and B. The critical temperature of in-situ Al thin films are slightly enhanced over the bulk value of 1.2 K to near 1.5 K, due to thickness [13, 31]. The temperature dependence can be fitted with the generalized Kulik-Omelyanchuk relation [29] where $I_cR_N(\phi) = \frac{\alpha\Delta(T)}{2e} \frac{\sin(\phi)}{\sqrt{1-\tau\sin^2(\phi/2)}} \times \tanh\left[\frac{\Delta(T)}{2k_B T} \sqrt{1-\tau\sin^2(\phi/2)}\right]$. The actual I_cR_N is found by maximizing $I_cR_N(\phi)$ with respect to phase ϕ . $\Delta(T)$ is the BCS gap calculated using T_c of Al and τ is a measure of interface transparency with $\tau = 1$ being fully transparent. In the limit $T = 0$ and $\tau = 1$ we recover the relationship $I_cR_N = \alpha\Delta/e$. The equation fits sample B data best for $\alpha = 0.69\pi$ and $\tau = 1$ consistent with the values found from just the 100 nm JJ at 20mK. Thus temperature dependence of sample B also indicates a highly transparent interface.

The JJs are equipped with gates that allow the junction resistance to be varied up to a fully insulating state. Figure 5(b) shows the dependence of products I_cR_N and $I_{ex}R_N$ on gate voltage for the 100 nm JJ on sample B. The inset shows the dependence of R_N on gate voltage found from slope of IV curves at high current (black crosses) and differential resistance measured at $B_{\perp} = 110$ mT where Al is no longer superconducting. In the regime of high resistance and large current, nonlinearities can affect the extraction of R_N from the slope of IV outside the Al gap. The reliability of the extrapolation in the range plotted is confirmed by comparison of the extracted normal state resistance with resistance from gate voltage sweeps at $B_{\perp} = 110$ mT. While the density at zero gate voltage is taken from magnetotransport measurements on the same sample the JJ geometry does not allow for a dependable measurement of density for non-zero gate voltages. Previous studies of InAs 2DEG based devices have shown a small increase in I_cR_N with gate voltage [13, 33]. This feature is not present in our junction possibly due to the lower initial density of our samples. We observe a decrease of I_cR_N with applied gate voltage with $I_c = 0\mu A$ occurring at $R_N = 2.7$ k Ω .

In contrast to the decrease in I_cR_N , $I_{ex}R_N$ does not change appreciably with gate voltage, as previously observed with junctions of different lengths on sample B. At large negative gate voltages I_{ex} becomes very sensitive

to noise making extrapolation of the product $I_{ex}R_N$ difficult for high resistances. Consequently the most negative gate voltage used for measurement is $V_g = -8V$ where

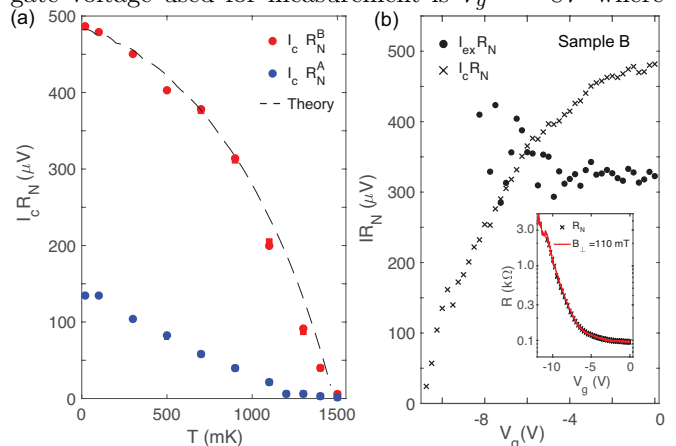


FIG. 5: (Color online) (a) Temperature dependence of the I_cR_N products for both samples. Dashed line indicates fitting $I_cR_N^B$ data with unity transparency formula, see text. (b) Gate dependence of products I_cR_N and $I_{ex}R_N$ are shown for 100 nm JJ on sample B. Inset shows gate dependence of junction R_N for same device. Black crosses show R_N from high current VI slope. Red line shows R_N measured at $B_{\perp} = 110$ mT where Al is not superconducting.

$R_N = 300$ Ω . The product $I_{ex}R_N$ at $V_g = -8$ V is found to be very similar to $V_g = 0$ V despite having three times the normal resistance. At $V_g = -8$ V, I_cR_N is about half its value at $V_g = 0$ V. This gate voltage independence further emphasizes that $I_{ex}R_N$ depends primarily on interface transparency which is unaffected by density changes in the 2DEG.

In conclusion we study Josephson junctions with in-situ epitaxial contact to InAs 2DEG's with different mobilities. We observe a remarkable difference in junction properties I_cR_N and $I_{ex}R_N$. Since both samples have in-situ epitaxial contact this difference is unexpected. One possible explanation is surface scattering, which is the primary scattering mechanism for these structures, contributing an extra component to scattering at the interface. These results indicate that just in-situ epitaxial contact does not guarantee a transparent interface. In the higher mobility sample for 100 nm JJ we find product $I_cR_N/\Delta_0 \sim 2.2$ which is the highest reported value of semiconductor based junction to our knowledge. Remarkably we observe $I_{ex}R_N \sim 1.5$ to be independent of both junction length and gate voltage in this sample. This is in contrast to previous studies which all see a decrease in $I_{ex}R_N$ and is the strongest indication of the highly transparent interface from in-situ epitaxial contact to a high mobility surface 2DEG.

-
- [1] J. Alicea, Reports on Progress in Physics **75**, 076501 (2012).
- [2] S. R. Elliott and M. Franz, Rev. Mod. Phys. **87**, 137 (2015).
- [3] Z. Qi, H. Xie, J. Shabani, V. E. Manucharyan, A. Levchenko, and M. G. Vavilov, Phys. Rev. B **97**, 134518 (2018).
- [4] L. Casparis, M. R. Connolly, M. Kjaergaard, N. J. Pearson, A. Kringhøj, T. W. Larsen, F. Kuemmeth, T. Wang, C. Thomas, S. Gronin, et al., Nature Nanotechnology **13**, 915 (2018).
- [5] T. W. Larsen, K. D. Petersson, F. Kuemmeth, T. S. Jespersen, P. Krogstrup, J. Nygård, and C. M. Marcus, Phys. Rev. Lett. **115**, 127001 (2015).
- [6] Z. Wan, A. Kazakov, M. J. Manfra, L. N. Pfeiffer, K. W. West, and L. P. Rokhinson, Nature Communications **6**, 7426 EP (2015).
- [7] T. D. Clark, R. J. Prance, and A. D. C. Grassie, Journal of Applied Physics **51**, 2736 (1980).
- [8] A. Richter, M. Koch, T. Matsuyama, and U. Merkt, Supercond. Sci. Technol. **12**, 874 (1999).
- [9] H. Kroemer, C. Nguyen, and E. L. Hu, Solid-State Electronics **37**, 1021 (1994).
- [10] H. Takayanagi and T. Akazaki, Solid State Communications **96**, 815 (1995), ISSN 0038-1098.
- [11] Y.-J. Doh, J. A. van Dam, A. L. Roest, E. P. A. M. Bakkers, L. P. Kouwenhoven, and S. D. Franceschi, Science **309**, 5732 (2005).
- [12] W. Chang, S. M. Albrecht, T. S. Jespersen, F. Kuemmeth, P. Krogstrup, J. Nygård, and C. M. Marcus, Nat Nano **10**, 232 (2015).
- [13] J. Shabani, M. Kjaergaard, H. J. Suominen, Y. Kim, F. Nichele, K. Pakrouski, T. Stankevic, R. M. Lutchyn, P. Krogstrup, R. Feidenhans'l, et al., Phys. Rev. B **93**, 155402 (2016).
- [14] J. P. Heida, B. J. van Wees, T. M. Klapwijk, and G. Borghs, Phys. Rev. B **60**, 13135 (1999).
- [15] J. D. Sau, S. Tewari, and S. Das Sarma, Phys. Rev. B **85**, 064512 (2012).
- [16] A. Haim and A. Stern, arXiv:1808.07886 (2018).
- [17] W. S. Cole, S. Das Sarma, and T. D. Stanescu, Phys. Rev. B **92**, 174511 (2015).
- [18] K. S. Wickramanighe, W. Mayer, J. Yuan, T. Nyugen, L. Jiao, V. Manucharyan, and J. Shabani, arXiv:1802.09569 (2018).
- [19] S. Abay, D. Persson, H. Nilsson, F. Wu, H. Q. Xu, M. Fogelstrom, V. Shumeiko, and P. Delsing, Phys. Rev. B **89**, 214508 (2014).
- [20] C. Li, S. G. nd A. Chepelianskii, and H. Bouchiat, Phys. Rev. B **94**, 115405 (2016).
- [21] P. Samuelsson, A. Ingerman, G. Johansson, E. V. Bezuglyi, V. Shumeiko, G. Wendin, R. Kursten, A. Richter, T. Matsuyama, and U. Merkt, Phys. Rev. B **70**, 212505 (2004).
- [22] X. Wallart, J. Lastennet, D. Vignaud, and F. Mollot, Appl. Phys. Lett. **87**, 043504 (2005).
- [23] J. Shabani, A. P. McFadden, B. Shojaei, and C. J. Palmstrøm, Applied Physics Letters **105**, 26 (2014).
- [24] V. Ambegaokar and A. Baratoff, Phys. Rev. Lett. **10**, 486 (1963).
- [25] K. K. Likharev, Rev. Mod. Phys. **51**, 101 (1979).
- [26] M. Kjaergaard, F. Nichele, H. J. Suominen, M. P. Nowak, M. Wimmer, A. R. Akhmerov, J. A. Folk, K. Flensberg, J. Shabani, C. J. Palmstrøm, et al., Nature Communications **7**, 12841 EP (2016).
- [27] G. E. Blonder, M. Tinkham, and T. M. Klapwijk, Phys. Rev. B **25**, 4515 (1982).
- [28] I. O. Kulik and A. N. Omelyanchuk, JETP Lett. **21**, 96 (1975).
- [29] K. A. Delin and A. W. Kleinsasser, Superconductor Science and Technology **9**, 227 (1996).
- [30] A. Ingerman, G. Johansson, V. S. Shumeiko, and G. Wendin, Phys. Rev. B **64**, 144504 (2001).
- [31] P. M. Tedrow and R. Meservey, Phys. Rev. B **25**, 171 (1982).
- [32] H. Courtois, M. Meschke, J. T. Peltonen, and J. P. Pekola, Phys. Rev. Lett. **101**, 067002 (2008).
- [33] M. Kjaergaard, H. J. Suominen, M. P. Nowak, A. R. Akhmerov, J. Shabani, C. J. Palmstrøm, F. Nichele, and C. M. Marcus, Phys. Rev. Applied **7**, 034029 (2017).